

ESVM : an open-source finite volume Electrostatic Vlasov-Maxwell code

Michaël J TOUATI^{1, 2, 3}

¹ Department of Electrical Engineering, University of California Los Angeles, Los Angeles, CA 90095, USA ² Group of Lasers and Plasmas, IPFN, IST, Universidade de Lisboa, Lisbon, Portugal ³ Centro de Láseres Pulsados de Salamanca (CLPU), Edificio M5, Parque Científico, C/ Adaja 8, 37185 Villamayor, Salamanca, Spain (current affiliation)

DOI: [10.21105/joss.03618](https://doi.org/10.21105/joss.03618)

Software

- [Review](#) ↗
- [Repository](#) ↗
- [Archive](#) ↗

Editor: [Daniel S. Katz](#) ↗

Reviewers:

- [@tclune](#)
- [@TomGoffrey](#)
- [@rouson](#)

Submitted: 11 August 2021

Published: 18 October 2021

License

Authors of papers retain copyright and release the work under a Creative Commons Attribution 4.0 International License ([CC BY 4.0](#)).

Summary

A plasma is a set of charged particles consisting of electrons and ionized atoms whose quantity is sufficiently large to behave collectively through the long-distance electromagnetic fields they produce. It is thought that more than 99.9% of visible matter in the Universe is in Plasma state. In a collisionless plasma consisting in an ionized gas composed of electrons moving in between much heavier ions, any electrostatic field is rapidly screened by the plasma electrons over the Debye screening distance ([Debye & Hückel, 1923](#)). When the number of electrons in these Debye spheres can be assumed to be infinite, the plasma electron population is correctly described by the Vlasov equation ([Vlasov, 1938](#)) that neglects all correlations between particles such as the binary Coulomb collisions between them. Besides its simplicity, the resulting Vlasov-Maxwell set of equations is extremely rich in Physics and has many applications ranging from Astrophysics and theoretical Plasma Physics to intense laser-matter interaction experiments. **ESVM** (ElectroStatic Vlasov-Maxwell) is a Vlasov-Maxwell Fortran 95 standard-compliant code, parallelized with OpenMP and using Python 3 for post-processing, that allows for the study of these collisionless plasmas. Many finite volume advection schemes ([Godunov, 1959](#)) are implemented in order to discretize the Vlasov equation, namely : - the donor-cell scheme, i.e. the downwind / upwind scheme ([R. Courant et al., 1952](#)) depending on the advection direction in each phase-space cell, - the Lax-Wendroff scheme ([Lax & Wendroff, 1960](#)), - the Fromm scheme ([Fromm, 1968](#)), - the Beam-Warming scheme ([Beam & Warming, 1976](#)), - the Van Leer scheme ([Van Leer, 1977](#)), - the minmod scheme ([Roe, 1986](#)), - the superbee scheme ([Roe, 1986](#)) and - two Monotonic Upwind-centered Scheme for Conservation Laws (MUSCL) ([van Leer, 1979](#)) schemes MUSCL2 ([Crouseilles & Filbet, 2004](#)) and MUSCL1 ([Duclos et al., 2009](#)).

Contrary to the linear second order Lax-Wendroff, Fromm and Beam-Warming schemes, the non-linear second order minmod, superbee, Van Leer and MUSCL schemes make use of a Total Variation Diminishing (TVD) non-linear flux limiter with the price of becoming a first order scheme in some phase-space cells to limit the numerical oscillations. The donor-cell scheme is a first order method and has the pros of limiting such eventual oscillations but the cons of being numerically less consistent and more diffusive. In ESVM, the discretized Vlasov equation is coupled with the self-consistent Maxwell-Gauss equation or equivalently with the Maxwell-Ampere equation with Maxwell-Gauss equation computed at the first time step, only. While the second order Maxwell-Gauss solver needs a computationally expensive inversion of a tridiagonal matrix for the computation of the Poisson equation, the Maxwell-Ampere equation solver makes use of a faster first order numerical scheme (in time). Both absorbing and periodic boundary conditions for both the particles and the fields are implemented. Python scripts, using the Matplotlib and Numpy packages, are provided to automatically extract and plot the stored simulation results. The simulation parameters are described in the [input-deck](#) and they

can be modified without having to recompile the code. Compilation rules can be modified in the [makefile](#) depending on the user compiler preferences. Classical Plasma Physics academic case simulations that need less than one CPU×hour each, tools for testing the compilation of the code and tools for checking the simulation parameters are provided.

Statement of need

ESVM has been developed in order to adapt simulations to specific Plasma Physics problems by choosing the more adequate finite volume numerical advection scheme in order to compute the Vlasov equation phase-space advection derivatives and to choose between computing the Maxwell-Gauss equation or the Maxwell-Ampere equation with Maxwell-Gauss equation computed at the first time step, only. The code aims at being used by the open-source Highly Parallel Computing (HPC) Plasma Physics community ranging from under or post-graduate students to teachers and researchers who usually use Particle-In-Cell (PIC) codes ([Dawson, 1962](#)) to study collisionless plasmas. Indeed, the PIC method may prohibit the study of Plasma Physical processes on large time scales and/or for very dense collisionless plasmas due to the statistical and numerical fluctuations of the computed quantities imposed by the use of a finite number of particles. Also, plasma instabilities naturally develop in PIC codes, seeded by the available fluctuations spatial spectrum k-vector for which the instability growth rate is maximum and some small amplitude Plasma Physical processes may be hidden under the fluctuations level. Compared to the many open source PIC codes such as [Smilei \(Derouillat et al., 2018\)](#) and semi-Lagrangian codes such as [vmf90 \(de Buyl, 2014\)](#), there is no open source finite volume Vlasov-Maxwell codes in the literature that are not based on an expansion method such as ([Tzoufras et al., 2011](#)), [AMORE \(Touati et al., 2014\)](#) or [Vlapy \(Joglekar & Levy, 2020\)](#). Finally, since the Vlasov equation is a conservation equation of the probable number of particles in the phase-space, using a finite volume method in order to compute the Vlasov equation presents the advantage of allowing for the use of numerical schemes that are numerically flux conserving and/or that ensure the distribution function positivity compared to other numerical methods. ESVM has already been used during courses for under and post-graduate students about the “numerical tools for laser-plasma interaction Physics” and it is currently used for theoretical Plasma Physics investigations.

Equations computed by ESVM

Plasma ions are assumed to be immobile with a homogeneous density n_i and fully ionized with an electrical charge Ze where Z is the plasma ion atomic number and e the elementary charge. The plasma electron distribution function $f_e(x, v_x, t)$ is computed by ESVM according to the plasma electron Vlasov equation

$$\frac{\partial f_e}{\partial t}(x, v_x, t) + \frac{\partial}{\partial x}(v_x f_e(x, v_x, t)) - \frac{\partial}{\partial v_x} \left(\frac{e}{m_e} E_x(x, t) f_e(x, v_x, t) \right) = 0 \quad (1)$$

that is self-consistently coupled with the Maxwell-Gauss equation

$$\frac{\partial E_x}{\partial x}(x, t) = 4\pi e (Zn_i - n_e(x, t)) \quad (2)$$

for the electrostatic field $E_x(x, t)$ or, equivalently, self-consistently coupled with the Maxwell-Ampere equation

$$\frac{\partial E_x}{\partial t}(x, t) = -4\pi j_e(x, t) \quad (3)$$

with Maxwell-Gauss equation [Equation 2](#) computed at the simulation start $t = 0$, only. Indeed, by integrating the plasma electron Vlasov equation [Equation 1](#) over the whole plasma electron

84 velocity space $v_x \in [v_{x,\min}, v_{x,\max}]$, one gets the hydrodynamic equation of plasma electron
85 number conservation

$$\frac{\partial n_e}{\partial t}(x, t) + \frac{\partial}{\partial x} (n_e v_e(x, t)) = 0, \quad (4)$$

86 which, when injected in the time derivative of Maxwell-Gauss equation Equation 2, provides
87 the Maxwell-Ampere equation Equation 3 if Maxwell-Gauss equation Equation 2 is verified at
88 the simulation start $t=0$. Here,

$$n_e(x, t) = \int_{v_{x,\min}}^{v_{x,\max}} f_e(x, v_x, t) dv_x, \quad (5)$$

89

$$v_e(x, t) = \frac{1}{n_e(x, t)} \int_{v_{x,\min}}^{v_{x,\max}} f_e(x, v_x, t) v_x dv_x \quad (6)$$

90 and

$$j_e(x, t) = -en_e(x, t)v_e(x, t) \quad (7)$$

91 are the plasma electron density, mean velocity and electrical charge current, respectively.
92 ESVM also computes the plasma electron thermal velocity $v_{T_e}(x, t)$ defined according to the
93 plasma electron internal energy density

$$u_{T_e}(x, t) = \frac{m_e}{2} n_e(x, t) v_{T_e}(x, t)^2 = \frac{m_e}{2} \int_{v_{x,\min}}^{v_{x,\max}} f_e(x, v_x, t) (v_x - v_e(x, t))^2 dv_x. \quad (8)$$

94 For example, in 1D plasmas at local Maxwell-Boltzmann equilibrium, $v_{T_e}(x, t) =$
95 $\sqrt{k_B T_e(x, t)/m_e}$ where k_B is the Boltzmann constant, $T_e(x, t)$ is the local electron
96 temperature and m_e is the electron mass. Maxwell-Gauss equation Equation 2 is computed
97 by using the electrostatic potential definition

$$\frac{\partial \Phi}{\partial x}(x, t) = -E_x(x, t) \quad (9)$$

98 that gives the Poisson equation

$$\frac{\partial^2 \Phi}{\partial x^2}(x, t) = -4\pi e (Zn_i - n_e(x, t)) \quad (10)$$

99 for the electrostatic potential Φ when injected in the Maxwell-Gauss equation Equation 2.
100 When the simulation is running, ESVM stores at every time steps and displays on the terminal
101 at every dumped time steps t_d the total plasma electron internal and kinetic energy (assuming
102 simulations with an area unit perpendicular to the x -axis of λ_{Debye}^2) and the total electrostatic
103 energy in the simulation box $x \in [x_{\min}, x_{\max}]$

$$U_{T_e}(t_d) = \lambda_{\text{Debye}}^2 \int_{x_{\min}}^{x_{\max}} u_{T_e}(x, t_d) dx, \quad (11)$$

104

$$U_{K_e}(t_d) = \lambda_{\text{Debye}}^2 \int_{x_{\min}}^{x_{\max}} \frac{m_e}{2} n_e(x, t) v_e(x, t_d)^2 dx \quad (12)$$

105 and

$$U_{E_x}(t_d) = \lambda_{\text{Debye}}^2 \int_{x_{\min}}^{x_{\max}} \frac{E_x(x, t_d)^2}{8\pi} dx, \quad (13)$$

106 respectively, as well as the total energy

$$U_{\text{tot}}(t_d) = U_{T_e}(t_d) + U_{K_e}(t_d) + U_{E_x}(t_d) \quad (14)$$

107 in order to check the energy conservation in the simulation. The user can initialize : - an
108 initial plasma electron population at Maxwell-Boltzmann equilibrium drifting at the velocity v_d
109

$$\begin{cases} f_e(x, v_x, t = 0) &= \frac{Zn_i}{\sqrt{2\pi v_{T_{e0}}^2}} \exp \left[-\frac{(v_x - v_d)^2}{2v_{T_{e0}}^2} \right] \\ E_x(x, t = 0) &= 0 \end{cases} \quad (15)$$

by no imposing any perturbation parameter or - a provided Plasma Physics academic case; cf. section **ESVM Plasma Physics academic case simulations**. - Finally, specific Plasma Physics simulations can easily be added in ESVM by implementing their initialization in the subroutines INIT_SIMU and/or DRIVE in the [library.f90](#) source file.

ESVM units

The code units consist in the commonly used electrostatic units : the electron mass m_e for masses, the elementary charge e for electrical charges, the inverse of the Langmuir plasma electron angular frequency $\omega_p = \sqrt{4\pi Z n_i e^2 / m_e}$ for times, the Debye electron screening length $\lambda_{\text{Debye}} = v_{T_{e_0}} / \omega_p$ and the average plasma electron density $n_0 = Z n_i$ for spatial densities. $v_{T_{e_0}}$ is therefore an important unit parameter of normalization since it fixes indirectly the space unit. It can be defined more generally as the initial plasma electron velocity distribution standard deviation if the plasma is not initialized at Maxwell-Boltzmann thermodynamic equilibrium [Equation 15](#); cf. [Equation 8](#). Injecting these units in the equations computed by the code, detailed in the previous section, one deduces the resulting normalized energies, electrostatic field, electrostatic potential, plasma electron electrical current and distribution function that consequently reads $\underline{U}_X = U_X / (n_0 \lambda_{\text{Debye}}^3 m_e v_{T_{e_0}}^2)$ where $X = T_e, K_e$ or $E_x, \underline{E}_x = e E_x / (m_e \omega_p v_{T_{e_0}})$, $\underline{\Phi} = e \Phi / (m_e v_{T_{e_0}}^2)$, $\underline{j}_e = j_e / (n_0 e v_{T_{e_0}})$ and $\underline{f}_e = f_e v_{T_{e_0}} / n_0$, respectively.

ESVM numerical stability

The spatial grid cells should be chosen lower than the Debye length $\Delta x < \lambda_{\text{Debye}}$ for the simulation to be Physical. $v_{x,\min}$ and $v_{x,\max}$ should be chosen sufficiently large $|v_{x,\min/\max}| \gg v_{T_{e_0}}$ in such a way that there is no plasma electrons outside the simulation velocity space during the whole simulation; cf. the continuity equation [Equation 4](#). The simulation velocity bin size should be chosen lower than the thermal electron velocity $\Delta v_x < v_{T_{e_0}}$ and also sufficiently small to capture the desired Physics. The CFL stability condition, from the name of its finder R. Courant, K. Friedrichs and H. Lewy ([R. Courant et al., 1928](#)), is implemented inside the code in such a way that the user just needs to specify in the input deck the scalar parameter $\text{cfl} < 1$ that fixes the normalized simulation time step according to

$$\Delta t_n = \text{cfl} \times F^n(\Delta x, \Delta v_x) < F^n(\Delta x, \Delta v_x) \quad (16)$$

at the time step $t_n = \sum_{m=1}^n \Delta t_m$ at time iteration n where $F^n(\Delta x, \Delta v_x)$ depends on the chosen numerical scheme. For example, if one notes

$$\underline{f}_e^{n,i}(v_x) = \frac{1}{\Delta x} \int_{x_{i-1/2}}^{x_{i+1/2}} \underline{f}_e(\underline{x}, v_x, t_n) d\underline{x} \quad (17)$$

the finite volume plasma electron distribution function at the phase-space bin located in between $x_{i-1/2} = x_i - \Delta x/2$ and $x_{i+1/2} = x_i + \Delta x/2$ and one considers the Lax-Wendroff method to compute the advection

$$\frac{\partial \underline{f}_e}{\partial t} + v_x \frac{\partial \underline{f}_e}{\partial x} = 0 \quad (18)$$

of plasma electrons along the spatial x -axis in the phase-space, the numerical scheme reads

$$\frac{\underline{f}_e^{n+1,i} - \underline{f}_e^{n,i}}{\Delta t_n} + v_x \frac{\underline{F}_x^{n,i+1/2} - \underline{F}_x^{n,i-1/2}}{\Delta x} = 0 \quad (19)$$

where the plasma electron fluxes across the bin volume interfaces located at $\underline{x}_{i\pm 1/2}$ are given by

$$\underline{F}_x^{n,i+1/2} = \frac{\underline{f}_e^{n,i+1} + \underline{f}_e^{n,i}}{2} - \frac{v_x \underline{\Delta t}_n}{\underline{\Delta x}} \frac{\underline{f}_e^{n,i+1} - \underline{f}_e^{n,i}}{2} \quad (20)$$

and

$$\underline{F}_x^{n,i-1/2} = \frac{\underline{f}_e^{n,i} + \underline{f}_e^{n,i-1}}{2} - \frac{v_x \underline{\Delta t}_n}{\underline{\Delta x}} \frac{\underline{f}_e^{n,i} - \underline{f}_e^{n,i-1}}{2}. \quad (21)$$

According to the Taylor expansion of $\underline{f}_e^{n,i+i}$, $\underline{f}_e^{n,i-i}$ and $\underline{f}_e^{n+1,i}$ close to $(\underline{x}_i, \underline{t}_n)$ up to the third order in space and time, one can check the Lax-Wendroff numerical consistency error is indeed of second order :

$$\begin{aligned} \epsilon^{n,i} &= \frac{\underline{f}_e^{n+1,i} - \underline{f}_e^{n,i}}{\underline{\Delta t}_n} + v_x \frac{\underline{F}_x^{n,i+1/2} - \underline{F}_x^{n,i-1/2}}{\underline{\Delta x}} - \left(\left. \frac{\partial \underline{f}_e}{\partial \underline{t}} \right|^{n,i} + v_x \left. \frac{\partial \underline{f}_e}{\partial \underline{x}} \right|^{n,i} \right) \\ &= \frac{\underline{\Delta t}_n^2}{6} \left. \frac{\partial^3 \underline{f}_e}{\partial \underline{t}^3} \right|^{n,i} + v_x \frac{\underline{\Delta x}^2}{6} \left. \frac{\partial^3 \underline{f}_e}{\partial \underline{x}^3} \right|^{n,i} + O(\underline{\Delta t}_n^3 + \underline{\Delta x}^3 + \underline{\Delta t}_n \underline{\Delta x}^2). \end{aligned} \quad (22)$$

By using the Von Neumann stability analysis, assuming periodic boundary conditions for simplicity and noting

$$\underline{\hat{f}}_e^n(\underline{k}^p) = \frac{1}{N_x} \sum_{i=1}^{N_x} \underline{f}_e^{n,i} \exp(-i \underline{k}^p \underline{x}_i) \Leftrightarrow \underline{f}_e^{n,i} = \sum_{p=1}^{N_x} \underline{\hat{f}}_e^n(\underline{k}^p) \exp(i \underline{k}^p \underline{x}_i) \quad (23)$$

with $\iota^2 = -1$, $N_x = 1 + (\underline{x}_{\max} - \underline{x}_{\min})/\underline{\Delta x}$ the number of spatial grid points and $\underline{k}^p = 2\pi(p-1)/(\underline{x}_{\max} - \underline{x}_{\min})$ the discrete Fourier mode, one gets by injecting Equation 23 in Equation 19

$$\frac{\underline{\hat{f}}_e^{n+1}(\underline{k}^p)}{\underline{\hat{f}}_e^n(\underline{k}^p)} = 1 - \frac{v_x \underline{\Delta t}_n}{\underline{\Delta x}} \iota \sin(\underline{k}^p \underline{\Delta x}) + \left(\frac{v_x \underline{\Delta t}_n}{\underline{\Delta x}} \right)^2 [\cos(\underline{k}^p \underline{\Delta x}) - 1] \quad (24)$$

for each term p of the series. It implies the numerical scheme is stable,

$$\text{meaning } \left| \frac{\underline{\hat{f}}_e^{n+1}(\underline{k}^p)}{\underline{\hat{f}}_e^n(\underline{k}^p)} \right| < 1, \text{ if } \underline{\Delta t}_n < \frac{\underline{\Delta x}}{v_x}. \quad (25)$$

Performing the same reasoning when also considering the advection of plasma electrons along the v_x -axis in the phase-space due to the action of the electrostatic field, with bins centered at $\underline{v}_x^\ell = \underline{v}_{x,\min} + (\ell-1)\underline{\Delta v}_x$ where $\ell \in [1, N_{v_x}]$ and $N_{v_x} = 1 + (\underline{v}_{x,\max} - \underline{v}_{x,\min})/\underline{\Delta v}_x$, in order to compute the Vlasov equation Equation 1 and update all $\underline{f}_e^{n,i,\ell}$ with each numerical scheme implemented in ESVM, one finds (sometimes empirically when it is too difficult analytically) that

$$F^n(\underline{\Delta x}, \underline{\Delta v}_x) = \frac{1/2}{\frac{\max_{\ell \in [1, N_{v_x}]} \{v_x^\ell\}}{\underline{\Delta x}} + \frac{\max_{i \in [1, N_x]} \{E_x^{n,i}\}}{\underline{\Delta v}_x}}. \quad (26)$$

is a sufficient CFL stability condition for all numerical schemes implemented in ESVM to be stable.

ESVM Plasma Physics academic case simulations

Four well-known Plasma Physics academic cases are provided with ESVM : 1) the emission of an electrostatic wakefield by a Gaussian electron; cf. Figure 1 2) the linear Landau damping of

167 an electron plasma wave; cf. Figure 2, 3) the non-linear Landau damping of an electron plasma
 168 wave; cf. Figure 3 and 4) the two-stream instability of two counter-propagating symmetric
 169 Gaussian electron beams; cf. Figure 4.

170 For each academic case, an example of input deck is provided together with one corresponding
 171 simulation result plot that the code typically generates. For 1), 2) and 3), the simulation is
 172 initialized assuming a non-drifting collisionless plasma at Maxwell-Boltzmann equilibrium

$$\begin{cases} f_e^{(0)}(x, v_x, t = 0) &= \frac{Zn_i}{\sqrt{2\pi v_{Te_0}^2}} \exp\left[-\frac{v_x^2}{2v_{Te_0}^2}\right] \\ E_x^{(0)}(x, t = 0) &= 0 \end{cases} \quad (27)$$

173 that is perturbed : - with a small perturbation

$$\delta f_e(x, v_x, t = 0) = A \frac{Zn_i}{2\pi\delta x\delta v} \exp\left[-\frac{(x-x_d)^2}{2\delta x^2}\right] \exp\left[-\frac{(v_x-v_d)^2}{2\delta v^2}\right], \quad (28)$$

174 consisting in a Gaussian electron located at $x_d = x_{\min} + (x_{\max} - x_{\min})/8$ with a standard
 175 deviation $\delta x = \lambda_{\text{Debye}}/4$ and drifting at a velocity v_d with a standard deviation $\delta v = v_{Te_0}/40$
 176 at the simulation start $t = 0$ for 1), and - with a small perturbation consisting in a small
 177 amplitude electron plasma wave

$$\delta E_x(x, t < \delta t) = A \frac{m_e \omega_p v_{Te_0}}{e} \sin(\omega_0 t - kx) \quad (29)$$

178 propagating during a short time interval $\delta t = 6\pi/\omega_0$ after the simulation start $t = 0$ for 2)
 179 and 3).

180 Only the perturbation amplitudes $A < 1$ for 1), 2) and 3), the perturbation drift velocity
 181 $v_d > v_{Te_0}$ for 1) and the perturbation temporal and spatial angular frequencies ω_0 and k for
 182 2) and 3) should be modified by the user when filling the input-deck in such a way that

$$\begin{cases} f_e(x, v_x, t) &= f_e^{(0)}(x, v_x, t) + \delta f_e(x, v_x, t) \\ E_x(x, t) &= E_x^{(0)}(x, t) + \delta E_x(x, t) \end{cases} \quad \text{with } |\delta f_e(x, v_x, t)| \ll f_e^{(0)}(x, v_x, t) \quad (30)$$

183 keeps being respected during the linear stage of the simulation. Except for non-linear Plasma
 184 Physics processes such as 3) for which the non-linear theory should be considered (Sagdeev
 185 & Galeev, 1969), the methodology that can be used to check any ESVM simulation results is
 186 always the same. Only analytical estimates used to check the ESVM simulation results of the
 187 provided academic case 4) are consequently detailed here in order to highlight it. The user can
 188 check the provided academic case simulation results 1), 2) and 3) by directly comparing the
 189 ESVM simulation results with the analytical estimates provided in (Decyk, 1987) (available
 190 at <https://picksc.idre.ucla.edu/wp-content/uploads/2015/04/DecykKyiv1987.pdf>) and in the
 191 reference textbooks (Landau & Lifshitz, 1981) and (Sagdeev & Galeev, 1969), respectively.

192 The provided Plasma Physics academic case 4) is initialized assuming two counter-propagating
 193 homogeneous Gaussian electron beams 'e, +' and 'e, -' of exactly opposite drift velocity $\pm v_d$
 194 with same standard deviation v_{Te_0}

$$f_e^{(0)}(x, v_x, t) = f_{e,+}^{(0)}(x, v_x, t) + f_{e,-}^{(0)}(x, v_x, t) \quad (31)$$

195 with

$$f_{e,\pm}^{(0)}(x, v_x, t) = \frac{Zn_i/2}{\sqrt{2\pi v_{Te_0}^2}} \exp\left[-\frac{(v_x \mp v_d)^2}{2v_{Te_0}^2}\right] \quad (32)$$

196 that is a solution of the Vlasov Equation Equation 1 and that doesn't produce any electrostatic
 197 fields

$$E_x^{(0)}(x, t) = 0 \quad (33)$$

198 according to Maxwell-Gauss Equation Equation 2. If one computes the Vlasov-Maxwell set
199 of Equations {Equation 1, Equation 2} exactly, initializing it with the two-stream equilibrium
200 distribution function Equation 31 without any perturbation, the counter-propagating elec-
201 tron beams would continue their propagation through the immobile plasma ions without any
202 modification. In order to observe the two-stream instability,

$$f_e(x, v_x, t = 0) = f_e^{(0)}(x, v_x, t = 0) + \delta f_e(x, v_x, t = 0), \quad (34)$$

203 is initialized instead by adding a small perturbation

$$\delta f_e(x, v_x, t = 0) = \delta f_{e,+}(x, v_x, t = 0) + \delta f_{e,-}(x, v_x, t = 0) \quad (35)$$

204 on each beam of the form

$$\delta f_{e,\pm}(x, v_x, t = 0) = \pm A \sin(k_1 x) f_{e,\pm}^{(0)}(x, v_x, t = 0) \quad (36)$$

205 at the simulation start $t = 0$ with $A = 0.1$ and $k_1 = 2\pi/L_x$ (parameter k in the input-deck)
206 that can be modified by the user in the input-deck where $L_x = x_{\max} - x_{\min}$.

207 In order to get analytical estimates of the exponentially growing electrostatic field, plasma
208 electron density and mean velocity perturbations in this ESVM simulation, one can linearize
209 the Vlasov equation Equation 1 and the self-consistent Maxwell-Gauss equation Equation 2
210 computed by ESVM assuming the perturbation Equation 35 remains small compared to the
211 equilibrium distribution Equation 31 during the simulation. They read

$$\frac{\partial \delta f_e}{\partial t} + \frac{\partial}{\partial x}(v_x \delta f_e) - \frac{e}{m_e} \frac{df_e^{(0)}}{dv_x} \delta E_x = 0 \quad (37)$$

212 and

$$\frac{\partial \delta E_x}{\partial x} = -4\pi e \int_{-\infty}^{\infty} \delta f_e dv_x, \quad (38)$$

213 up to the first order. Considering periodic boundary conditions, we may use a one-sided
214 Fourier transformation in time (thus equivalent to a Laplace transform) and a Fourier series
215 expansion in space for such a L_x -periodic initial condition problem. We will note

$$\hat{X}_p(t) = \frac{1}{L_x} \int_0^{L_x} X(x, t) \exp(+ik_p x) dx \Leftrightarrow X(x, t) = \sum_{p=-\infty}^{\infty} \hat{X}_p(t) \exp(-ik_p x) \quad (39)$$

216 with $\forall p \in \mathbb{Z}, k_p = 2\pi p/L_x$ and

$$\begin{aligned} \hat{\hat{X}}_p^{(+)}(\omega) &= \int_0^{\infty} dt \hat{X}_p(t) \exp(-i\omega t) \\ &= \int_0^{\infty} dt \int_0^{L_x} \frac{dx}{L_x} X(x, t) \exp[-i(\omega t - k_p x)] \\ \Leftrightarrow X(x, t) &= \int_{\iota R - \infty}^{\iota R + \infty} \frac{d\omega}{2\pi} \sum_{p=-\infty}^{\infty} \hat{\hat{X}}_p^{(+)}(\omega) \exp[+i(\omega t - k_p x)] \end{aligned} \quad (40)$$

217 where the integral in the complex ω -plane is taken along a straight line $\omega = \iota R$. By multiplying
218 Equation 37 and Equation 38 by $\exp[-i(\omega t - k_p x)]/L_x$ and by integrating them from $x = 0$
219 to $x = L_x$ and from $t = 0$ to $t = \infty$, we obtain respectively

$$\hat{\hat{f}}_{e,p}^{(+)} = \frac{1}{\iota(\omega - k_p v_x)} \left[\hat{\hat{f}}_{e,p}(v_x, t = 0) + \frac{e}{m_e} \frac{df_e^{(0)}}{dv_x} \hat{\hat{E}}_{x,p}^{(+)} \right] \quad (41)$$

220 with

$$\hat{\hat{f}}_{e,p}(v_x, t = 0) = \alpha_p A \frac{Z n_i / 2}{\sqrt{2\pi v_{Te_0}^2}} \left\{ \exp \left[-\frac{(v_x - v_d)^2}{2v_{Te_0}^2} \right] - \exp \left[-\frac{(v_x + v_d)^2}{2v_{Te_0}^2} \right] \right\} \quad (42)$$

221 where

$$\alpha_p = \begin{cases} \mp 1/2\iota & \text{if } p = \pm 1 \\ 0 & \text{else} \end{cases} \quad (43)$$

222 and

$$\widehat{\widehat{\mathbf{E}}}_{x,p}^{(+)} = \frac{4\pi e}{\iota k_p} \int_{-\infty}^{\infty} \widehat{\mathbf{f}}_{e,p}^{(+)}(\omega, v_x) dv_x. \quad (44)$$

223 Injecting Equation 41 in Equation 44, we obtain the Fourier components of the electrostatic
224 field Laplace transform

$$\begin{aligned} \widehat{\widehat{\mathbf{E}}}_{x,p}^{(+)}(\omega) &= \frac{4\pi e}{k_p^2 \epsilon(\omega, k_p)} \int_{-\infty}^{\infty} \frac{\widehat{\mathbf{f}}_{e,p}(v_x, t=0)}{v_x - \omega/k_p} dv_x \\ &= \alpha_p \frac{A}{2\sqrt{2}} \frac{m_e v_{Te_0}}{e} \frac{\mathcal{Z}\left(\frac{\omega/k_p - v_d}{v_{Te_0}\sqrt{2}}\right) - \mathcal{Z}\left(\frac{\omega/k_p + v_d}{v_{Te_0}\sqrt{2}}\right)}{\epsilon(\omega, k_p) (k_p \lambda_{\text{Debye}})^2} \end{aligned} \quad (45)$$

225 where the plasma electrical permittivity reads

$$\begin{aligned} \epsilon(\omega, k) &= 1 - \frac{4\pi e^2}{m_e k^2} \int_{-\infty}^{\infty} \frac{1}{v_x - \omega/k} \frac{df_e^{(0)}}{dv_x} dv_x \\ &= 1 + \frac{1}{(k \lambda_{\text{Debye}})^2} \left\{ 1 + \frac{1}{2} \left[F\left(\frac{\omega/k - v_d}{v_{Te_0}\sqrt{2}}\right) + F\left(\frac{\omega/k + v_d}{v_{Te_0}\sqrt{2}}\right) \right] \right\} \end{aligned} \quad (46)$$

226 depending on the plasma dispersion function (Fried & Conte, 1961)

$$F(\zeta) = \zeta \mathcal{Z}(\zeta) \text{ and } \mathcal{Z}(\zeta) = \frac{1}{\sqrt{\pi}} \int_{-\infty}^{\infty} \frac{\exp(-z^2)}{z - \zeta} dz. \quad (47)$$

227 Since $v_d \gg v_{Te_0}$ in this ESVM simulation, we have the condition

$$\left| \frac{\omega}{k_p} \pm v_d \right| \gg v_{Te_0} \sqrt{2} \quad (48)$$

228 that is fulfilled for any given spatial frequency mode k_p and one thus may use the asymptotic
229 limit

$$F(\zeta) \Big|_{|\zeta| \gg 1} = \iota \zeta \sqrt{\pi} \exp(-\zeta^2) - 1 - \frac{1}{2\zeta^2} - \frac{3}{4\zeta^4} + O\left(\frac{1}{\zeta^6}\right) \quad (49)$$

230 that leads to the simpler dispersion relation

$$\epsilon(\omega, k) \Big|_{v_d \gg v_{Te_0}} = 1 - \frac{\omega_p^2}{2} \left[\frac{1}{(\omega - kv_d)^2} + \frac{1}{(\omega + kv_d)^2} \right] = 0 \quad (50)$$

231 retaining only the main term in the series expansion of the dispersion function Equation 47
232 up to the second order Equation 49. In this limit, the dispersion relation Equation 50 provides
233 four pure real solutions $\{\omega_1(k), \omega_2(k), \omega_3(k), \omega_4(k)\} \in \mathbb{R}^4$ for wavenumber k greater
234 or equal than the critical wavenumber ω_p/v_d . It means that the two counter-propagating
235 electron beams remain stable on space scales smaller than $2\pi v_d/\omega_p$. However, in the case
236 where $k_p < \omega_p/v_d$ considered here, one finds in addition to the two real poles

$$\omega_{1/2}\left(k < \frac{\omega_p}{v_d}\right) = \pm \omega_0(k) \quad (51)$$

237 where

$$\omega_0(k) = \omega_p \sqrt{\left(\frac{kv_d}{\omega_p}\right)^2 + \frac{1}{2} \left(1 + \sqrt{1 + 8\left(\frac{kv_d}{\omega_p}\right)^2}\right)} \underset{kv_d \ll \omega_p}{\sim} \omega_p, \quad (52)$$

two another pure imaginary conjugate poles

$$\omega_{3/4}(k < k_c) = \pm i\delta(k). \quad (53)$$

It means that the two counter-propagating electron beams streaming through the immobile plasma ions are unstable on space scales greater than $2\pi v_d/\omega_p$ and that this two-stream instability grows exponentially at the rate

$$\delta(k) = \omega_p \sqrt{\frac{1}{2} \left(\sqrt{1 + 8 \left(\frac{kv_d}{\omega_p} \right)^2} - 1 \right) - \left(\frac{kv_d}{\omega_p} \right)^2} \sim_{kv_d \ll \omega_p} |k| v_d. \quad (54)$$

The stable electron plasma waves angular frequency Equation 52 and the two stream instability growth rate Equation 54 are plotted in Figure 5 as a function of the angular spatial frequency mode k . Retaining the main terms in the series expansions of \mathcal{Z} up to the second order in Equation 45 according to Equation 49, the Fourier components of the electrostatic field Laplace transform simplify into

$$\widehat{\delta E}_{x,p}^{(+)}(\omega) \sim_{v_d \gg v_{Te0}} -\alpha_p A \frac{m_e v_d}{e} \frac{\omega_p^2}{\epsilon(\omega, k_p)(\omega - k_p v_d)(\omega + k_p v_d)}. \quad (55)$$

The poles of the Fourier components of the electrostatic fields Equation 55 are thus $\pm k_p v_d$ plus the ones of the plasma electrical permittivity Equation 50 given by Equations 51 and Equation 53. We can now determine the time dependence of the spatial Fourier components of the growing electrostatic field

$$\widehat{\delta E}_{x,p}(t) = \frac{1}{2\pi} \int_{\iota R - \infty}^{\iota R + \infty} \widehat{\delta E}_{x,p}^{(+)}(\omega) \exp(+i\omega t) d\omega \quad (56)$$

by using the residue theorem with the contour illustrated in Figure 6 in order to evaluate the Cauchy principal value of this integral : since the function to integrate in Equation 56 is an analytic function of ω defined in the whole complex plane, we moved the contour of integration usually taken slightly above the real axis into the lower half-plane sufficiently far beneath the pole $-i\delta$ and passing round this pole and round the other poles lying above it in such a way that it doesn't cross any of the poles of the function. We thus obtain

$$\begin{aligned} \widehat{\delta E}_{x,p}(t) = & A E_0 \alpha_p \frac{\omega_p}{\delta(k_p)} \frac{\delta(k_p)^2 + (k_p v_d)^2}{\delta(k_p)^2 + \omega_0(k_p)^2} \sinh[\delta(k_p)t] \\ & + A \frac{E_0}{2} \alpha_p \frac{\omega_p}{\omega_0(k_p)} \frac{\omega_0(k_p)^2 - (k_p v_d)^2}{\delta(k_p)^2 + \omega_0(k_p)^2} \sin[\omega_0(k_p)t] \end{aligned} \quad (57)$$

with

$$E_0 = \frac{m_e v_d \omega_p}{e} \quad (58)$$

that finally gives according to the Fourier series expansion Equation 39

$$\begin{aligned} \delta E_x(x, t) = & A E_0 \frac{\omega_p}{\delta(k_1)} \frac{\delta(k_1)^2 + (k_1 v_d)^2}{\delta(k_1)^2 + \omega_0(k_1)^2} \sinh[\delta(k_1)t] \sin(k_1 x) \\ & + A \frac{E_0}{2} \frac{\omega_p}{\omega_0(k_1)} \frac{\omega_0(k_1)^2 - (k_1 v_d)^2}{\delta(k_1)^2 + \omega_0(k_1)^2} \sin[\omega_0(k_1)t] \sin(k_1 x). \end{aligned} \quad (59)$$

Knowing the electrostatic field Equation 59, one may also deduce the perturbed distribution

function according to Equation 37. It reads

$$\begin{aligned}\delta f_e(x, v_x, t) &= \delta f_e(x, v_x, t=0) + \frac{e}{m_e} \frac{df_e^{(0)}}{dv_x}(v_x) \int_0^t \delta E_x[x + v_x(\tau - t), \tau] d\tau \\ &= f_{e,+}^{(0)}(v_x) \left[A \sin(k_1 x) + \frac{v_d - v_x}{v_{Te0}^2} \frac{e}{m_e} \int_0^t \delta E_x[x + v_x(\tau - t), \tau] d\tau \right] \\ &+ f_{e,-}^{(0)}(v_x) \left[-A \sin(k_1 x) - \frac{v_d + v_x}{v_{Te0}^2} \frac{e}{m_e} \int_0^t \delta E_x[x + v_x(\tau - t), \tau] d\tau \right].\end{aligned}\quad (60)$$

In the limit $k_p v_d \ll \omega_p$, they simplify into

$$\delta E_x(x, t) \underset{k_1 v_d \ll \omega_p}{\sim} A \frac{E_0}{2} \left[\sin(\omega_p t) + 4 \frac{k_1 v_d}{\omega_p} \sinh(k_1 v_d t) \right] \sin(k_1 x) \quad (61)$$

and

$$\begin{aligned}\underset{k_1 v_d \ll \omega_p}{\sim} & A \frac{v_d}{1 - \left(\frac{k_1 v_x}{\omega_p}\right)^2} \left\{ \frac{e}{m_e} \int_0^t \delta E_x[x + v_x(\tau - t), \tau] d\tau \right. \\ & \left. \frac{k_1 v_x}{\omega_p} \sin(\omega_p t) \cos(k_1 x) - [\cos(\omega_p t) - 1] \sin(k_1 x) \right\} \\ + & A \frac{v_d}{1 + \left(\frac{v_x}{v_d}\right)^2} \left\{ -\frac{v_x}{v_d} \sinh(k_1 v_d t) \cos(k_1 x) + [\cosh(k_1 v_d t) - 1] \sin(k_1 x) \right\}.\end{aligned}\quad (62)$$

We thus deduce in this limit

$$\begin{aligned}\delta n_e(x, t) &= \int_{-\infty}^{\infty} \delta f_e(x, v_x, t) dv_x \\ &\underset{k_1 v_d \ll \omega_p}{\sim} -\frac{A}{2} Z n_i \frac{k_1 v_d}{\omega_p} \left[\sin(\omega_p t) + 4 \frac{k_1 v_d}{\omega_p} \sinh(k_1 v_d t) \right] \cos(k_1 x)\end{aligned}\quad (63)$$

and

$$\begin{aligned}\delta v_e(x, t) &= \frac{1}{Z n_i} \int_{-\infty}^{\infty} v_x \delta f_e(x, v_x, t) dv_x \\ &\underset{k_1 v_d \ll \omega_p}{\sim} -\frac{A}{2} v_d \left[(\cos(\omega_p t) - 1) + \left(2 \frac{k_1 v_d}{\omega_p}\right)^2 (\cosh(k_1 v_d t) - 1) \right] \sin(k_1 x).\end{aligned}\quad (64)$$

The first term in the square brackets

$$\begin{cases} \delta n_{\text{osc}}(x, t) \underset{k_1 v_d \ll \omega_p}{\sim} -\frac{A}{2} Z n_i \frac{k_1 v_d}{\omega_p} \sin(\omega_p t) \cos(k_1 x) \\ \delta v_{\text{osc}}(x, t) \underset{k_1 v_d \ll \omega_p}{\sim} -\frac{A}{2} v_d (\cos(\omega_p t) - 1) \sin(k_1 x) \\ \delta E_{\text{osc}}(x, t) \underset{k_1 v_d \ll \omega_p}{\sim} \frac{A}{2} E_0 \sin(\omega_p t) \sin(k_1 x) \end{cases} \quad (65)$$

corresponds to space-charge oscillations of stationary electrostatic plasma waves excited by the perturbation imposed on each electron beam. We are rather interested here in the second term in the square brackets

$$\begin{cases} \delta n_{\text{ins}}(x, t) \underset{k_1 v_d \ll \omega_p}{\sim} -2A Z n_i \left(\frac{k_1 v_d}{\omega_p}\right)^2 \sinh(k_1 v_d t) \cos(k_1 x) \\ \delta v_{\text{ins}}(x, t) \underset{k_1 v_d \ll \omega_p}{\sim} -2A v_d \left(\frac{k_1 v_d}{\omega_p}\right)^2 (\cosh(k_1 v_d t) - 1) \sin(k_1 x) \\ \delta E_{\text{ins}}(x, t) \underset{k_1 v_d \ll \omega_p}{\sim} 2A E_0 \frac{k_1 v_d}{\omega_p} \sinh(k_1 v_d t) \sin(k_1 x) \end{cases} \quad (66)$$

corresponding to the exponentially growing electrostatic field due to the two-stream instability. These latter growing electron density, current density and electrostatic field perturbations Equation 66 can directly be compared with the ESVM simulation result. One can also check that if $A = 0$, all quantities cancel. That confirms that, contrary to PIC codes, the two counter-propagating electron beams would continue their propagation without any modification if we do not impose an initial perturbation on which the instability will grow in ESVM. Finally, one can estimate the trajectories (x_ℓ, v_ℓ) of one beam electron $\ell \in [1, N_e]$ with an arbitrary initial velocity $v_\ell(t=0) = v_0$ in the beam velocity distribution function and an initial position $x_\ell(t=0) = x_0$ close to $x = 0$ such that $k_1 x_0 \ll 1$. At the early stage of the instability, the growing electrostatic field component δE_{ins} is small compared to the stationary plasma wave δE_{osc} that oscillates in time at the Langmuir electron angular frequency ω_p . On such time scale $\omega_p t \sim 1$, the beam electrons are consequently mainly affected by this electrostatic field component

$$m_e \frac{dv_\ell}{dt} = -e\delta E_{\text{osc}}(x_\ell(t), t) \quad (67)$$

and their trajectory is thus given by

$$\frac{d^2 x_\ell}{dt^2} + \omega_p^2 \left(\frac{A k_1 v_d}{2 \omega_p} \right) \sin(\omega_p t) x_\ell(t) = 0, \quad (68)$$

assuming that $k_1 x_\ell(t) \ll 1$ remains valid at every time $t > 0$ if it is valid at $t = 0$ such that $\forall t, \sin[k_1 x_\ell(t)] \sim k_1 x_\ell(t)$. Recognizing the Mathieu Equation

$$\frac{d^2 x_\ell}{du^2} + [a - 2q \cos(2u)] x_\ell(u) = 0 \quad (69)$$

with $a = 0$ and $q = -Ak_1 v_d / \omega_p$ by doing the change of variable $u(t) = (-\pi/4) + (\omega_p t/2)$, we deduce

$$k_1 x_\ell(t) = k_1 x_c c_{e,0}[q, u(t)] + k_1 x_s s_{e,0}[q, u(t)] \quad (70)$$

and

$$v_\ell(t) = \frac{v_d}{2} \frac{\omega_p}{k_1 v_d} \{k_1 x_c c'_{e,0}[q, u(t)] + k_1 x_s s'_{e,0}[q, u(t)]\} \quad (71)$$

with

$$\begin{cases} k_1 x_c = + \frac{s'_{e,0}(q, -\pi/4) k_1 x_0 - s_{e,0}(q, -\pi/4) (2k_1 v_d / \omega_p) (v_0 / v_d)}{c_{e,0}(q, -\pi/4) s'_{e,0}(q, -\pi/4) - c'_{e,0}(q, -\pi/4) s_{e,0}(q, -\pi/4)} \\ k_1 x_s = - \frac{c'_{e,0}(q, -\pi/4) k_1 x_0 - c_{e,0}(q, -\pi/4) (2k_1 v_d / \omega_p) (v_0 / v_d)}{c_{e,0}(q, -\pi/4) s'_{e,0}(q, -\pi/4) - c'_{e,0}(q, -\pi/4) s_{e,0}(q, -\pi/4)} \end{cases}, \quad (72)$$

accounting for the initial conditions at $t = 0$. Here, $c_{e,a}(q, u)$ and $s_{e,a}(q, u)$ are respectively the even and odd solutions of Mathieu Equation Equation 69 and $c'_{e,a}(q, u)$ and $s'_{e,a}(q, u)$ their first order derivatives. According to Equation 70 and Equation 71, the beam electron trajectories in space are only slightly modified compared to their ballistic initial trajectory $x_0 + v_0 t$ with a velocity that oscillates around their initial value v_0 with amplitudes slightly increasing with time. As a consequence, each beam velocity dispersion slightly increases with its propagation distance until the growing component of the electrostatic field δE_{ins} becomes greater than δE_{osc} . When this occurs, the equation of motion

$$m_e \frac{dv_\ell}{dt} = -e\delta E_{\text{ins}}(x_\ell(t), t) \quad (73)$$

gives

$$\frac{1}{2} \left(\frac{v_\ell(t)}{v_d} \right)^2 - \frac{1}{2} \left(\frac{v_0}{v_d} \right)^2 = -2Ak_1 \int_0^t v_\ell(t) \sin[k_1 x_\ell(t)] \sinh(k_1 v_d t) dt \quad (74)$$

and

$$\frac{d^2 x_\ell}{dt^2} + 2k_1 v_d^2 \sinh(k_1 v_d t) \sin[k_1 x_\ell(t)] = 0. \quad (75)$$

The energy conservation Equation Equation 74 shows that, at the early stage of the instability, electrons having a positive velocity $v_\ell(t) > 0$ at a location $0 < x_\ell(t) < L_x/2$ as well as electrons having a negative velocity $v_\ell(t) < 0$ at a location $-L_x/2 < x_\ell(t) < 0$ are losing energy contrary to electrons having a negative velocity $v_\ell(t) < 0$ at a location $0 < x_\ell(t) < L_x/2$ or electrons having a positive velocity $v_\ell(t) > 0$ at a location $-L_x/2 < x_\ell(t) < 0$ that are earning energy. In order to determine such an electron trajectory according to its equation of motion Equation 75, one can assume in addition that $k_1 x_\ell(t) \ll 1$ remains valid at every time $t > 0$ if it is valid at $t = 0$ such that $\forall t, \sin[k_1 x_\ell(t)] \sim k_1 x_\ell(t)$ and consider time scales of the order of electrostatic plasma oscillations ω_p^{-1} so that we may consider $\sinh(k_1 v_d t) \sim \exp(k_1 v_d t)/2$. In this case, Equation 75 simplifies into

$$\frac{d^2 x_\ell}{dt^2} + (k_1 v_d)^2 \exp(k_1 v_d t) x_\ell(t) = 0. \quad (76)$$

Recognizing the differential Bessel Equation by doing the change of variable $v(t) = \exp(k_1 v_d t)$

$$\frac{d^2 x_\ell}{dv^2} + \frac{1}{v} \frac{dx_\ell}{dv} + \frac{1}{v} x_\ell(v) = 0, \quad (77)$$

the beam electron trajectories can be found readily. They read

$$k_1 x_\ell(t) = k_1 x_J J_0(2\sqrt{v(t)}) + k_1 x_Y Y_0(2\sqrt{v(t)}) \quad (78)$$

and

$$v_\ell(t) = -v_d \left[k_1 x_J J_1(2\sqrt{v(t)}) + k_1 x_Y Y_1(2\sqrt{v(t)}) \right] \sqrt{v(t)} \quad (79)$$

with

$$\begin{cases} k_1 x_J &= + \frac{Y_1(2) k_1 x_0 + Y_0(2) (v_0/v_d)}{J_0(2) Y_1(2) - J_1(2) Y_0(2)} \\ k_1 x_Y &= - \frac{J_1(2) k_1 x_0 + J_0(2) (v_0/v_d)}{J_0(2) Y_1(2) - J_1(2) Y_0(2)} \end{cases}, \quad (80)$$

accounting for the initial conditions at $t = 0$. Here, J_μ and Y_μ are the Bessel functions of the first and second kind of order μ respectively. Some of these beam electron orbits are plotted in Figure 7. We can see that the beam electrons are looping around the phase-space center $(x, v) = (0, 0)$ with a velocity amplitude increasing with their initial spatial distance from $x = 0$ in agreement with the ESVM simulation Figure 4.

ESVM Perspectives

It is planned in a near future to : 1) provide another Plasma Physics academic simulation about one non-linear BGK electron plasma wave, from the name of its finder I. B. Bernstein, J. M. Greene and M. D. Kruskal (Bernstein et al., 1957) 2) provide another Plasma Physics academic simulation about the echo of two plasma electron waves (Gould et al., 1967) 3) implement non-equally spaced phase-space cells 4) implement high order Weighted Essentially Non-Oscillatory (WENO) advection schemes (Liu et al., 1994) 5) compute the plasma ion Vlasov equation to allow for the ions to be mobile 6) store the simulation results in hdf5 files instead of text files 7) implement MPI parallelization 8) implement vectorization 9) extend the code to the relativistic regime : ESVM \Rightarrow RESVM for open source Relativistic ElectroStatic Vlasov-Maxwell code 10) implement a BGK collision operator, from the name of its finder P. L. Bhatnagar, E. P. Gross and M. Krook (Bhatnagar et al., 1954) 11) extend the code to 1D-2V and 1D-3V phase-space electrostatic plasma simulations 12) implement the Landau (Landau, 1937) and Belaiev-Budker (Belaiev & Budker, 1956) relativistic collision operators using the Rosenbluth potentials (Rosenbluth et al., 1957) and their relativistic Braams-Karney extension (Braams & Karney, 1987) : (R)ESVM \Rightarrow (R)ESVFPM for open source (Relativistic) ElectroStatic Vlasov-Fokker-Planck-Maxwell code 13) extend the code to electrostatic 2D-1V,

2D-2V and 2D-3V phase-space plasma simulations : (R)ESV(FP)M \Rightarrow (R)ESV(FP)M2 for
open source (Relativistic) ElectroStatic Vlasov-(Fokker-Planck-)Maxwell in 2D 14) extend the
code with the second order finite difference Yee scheme (Yee, 1966) to electromagnetic 2D-1V,
2D-2V and 2D-3V phase-space plasma simulations : (R)ESV(FP)M(2) \Rightarrow (R)EMV(FP)M(2)
for open source (Relativistic) ElectroMagnetic Vlasov-(Fokker-Planck-)Maxwell (in 2D) 15)
implement the Perfectly Matched Layer (PML) technique (Berenger, 1994) to absorb the
electromagnetic fields at the spatial simulation box boundaries 16) deploy the code to GPU
architectures.

Figures

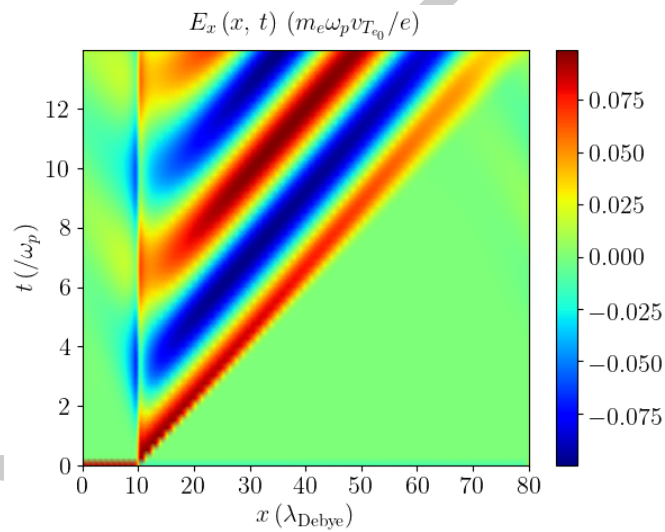


Figure 1: Electrostatic wakefield test case : Electrostatic wakefield $E_x(x, t)$ emitted by a Gaussian electron propagating in a collisionless plasma at Maxwell-Boltzmann equilibrium Equation 27 and initialized according to Equation 28 with $A = 0.1$ and $\underline{v}_d = 5$.

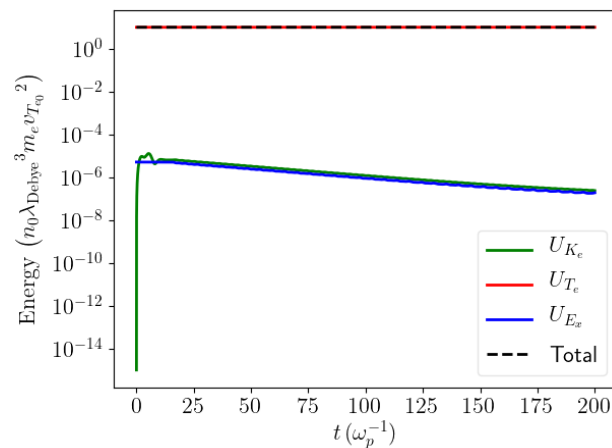


Figure 2: Linear Landau damping test case : Total electrostatic field energy and plasma electrons kinetic energy in the linearly Landau damped electron plasma wave propagating in the collisionless plasma at Maxwell-Boltzmann equilibrium Equation 27 and initialized according to Equation 29 with $A = 10^{-3}$, $\underline{k} = 0.29919930034$ and $\underline{\omega}_0 = 1.18$.

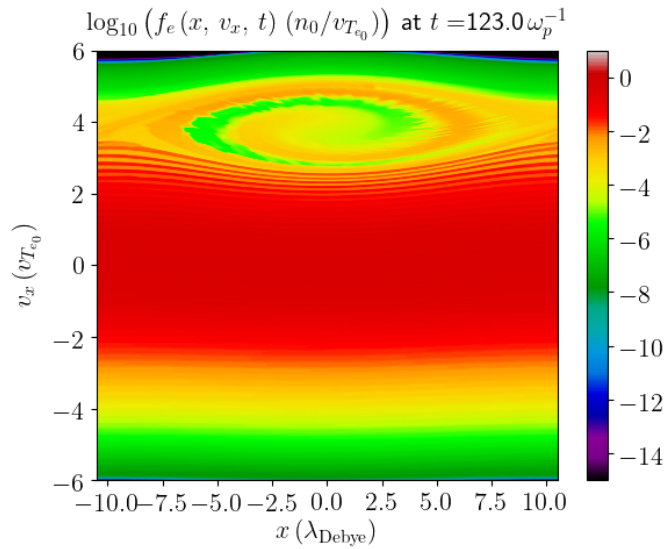


Figure 3: Non Linear Landau damping test case : Plasma electrons phase-space $f_e(x, v_x, \underline{t} = 68)$ in the non-linear Landau damping of the electron plasma wave propagating in the collisionless plasma at Maxwell-Boltzmann equilibrium Equation 27 and and initialized according to Equation 29 with $A = 10^{-1}$, $\underline{k} = 0.29919930034$ and $\underline{\omega}_0 = 1.18$.

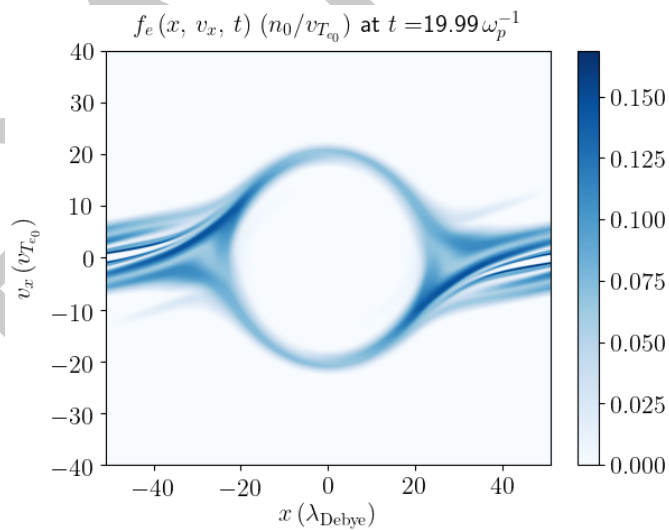


Figure 4: Two stream instability test case : Plasma electrons phase-space $f_e(x, v_x, \underline{t} = 19.99)$ in the two-stream instability of two counter-propagating electron beams initialized according to Equation 34 with $A = 10^{-1}$, $\underline{k} = 0.06159985595$ ($\underline{x}_{\min} = -\underline{x}_{\max} = 51$) and $\underline{v}_d = 10$.

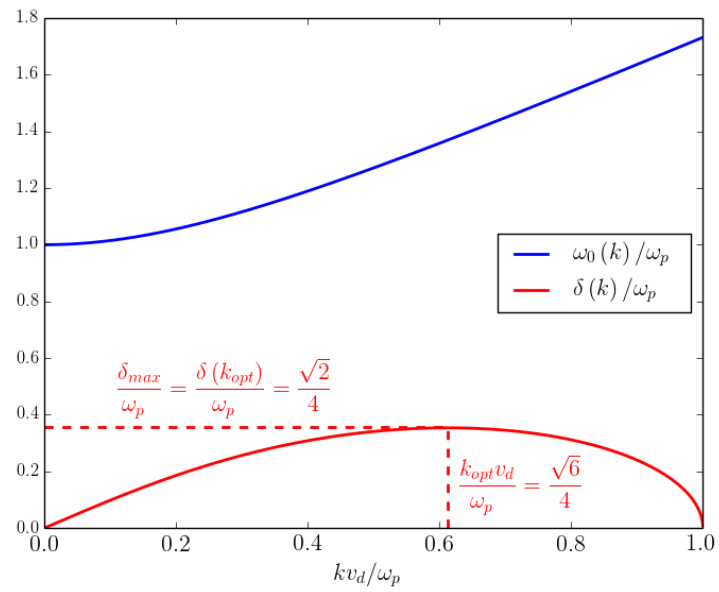


Figure 5: Two stream instability test case : Stationary electron plasma waves angular frequency Equation 52 and the two-stream instability growth rate Equation 54 as a function of the spatial angular frequency mode k .

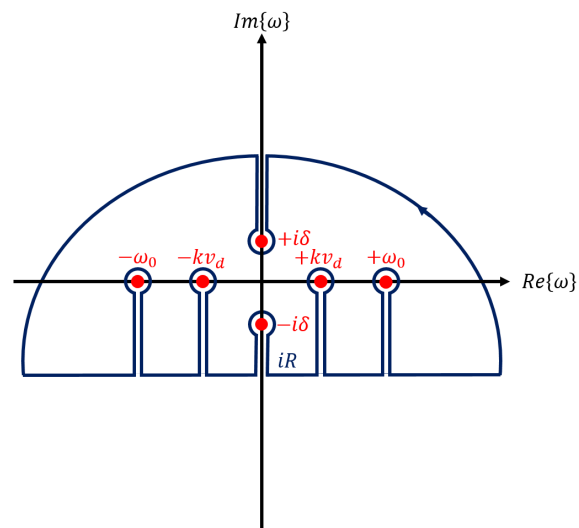


Figure 6: Two stream instability test case : Integration contour used to evaluate the the Cauchy principal value of the integral Equation 56.

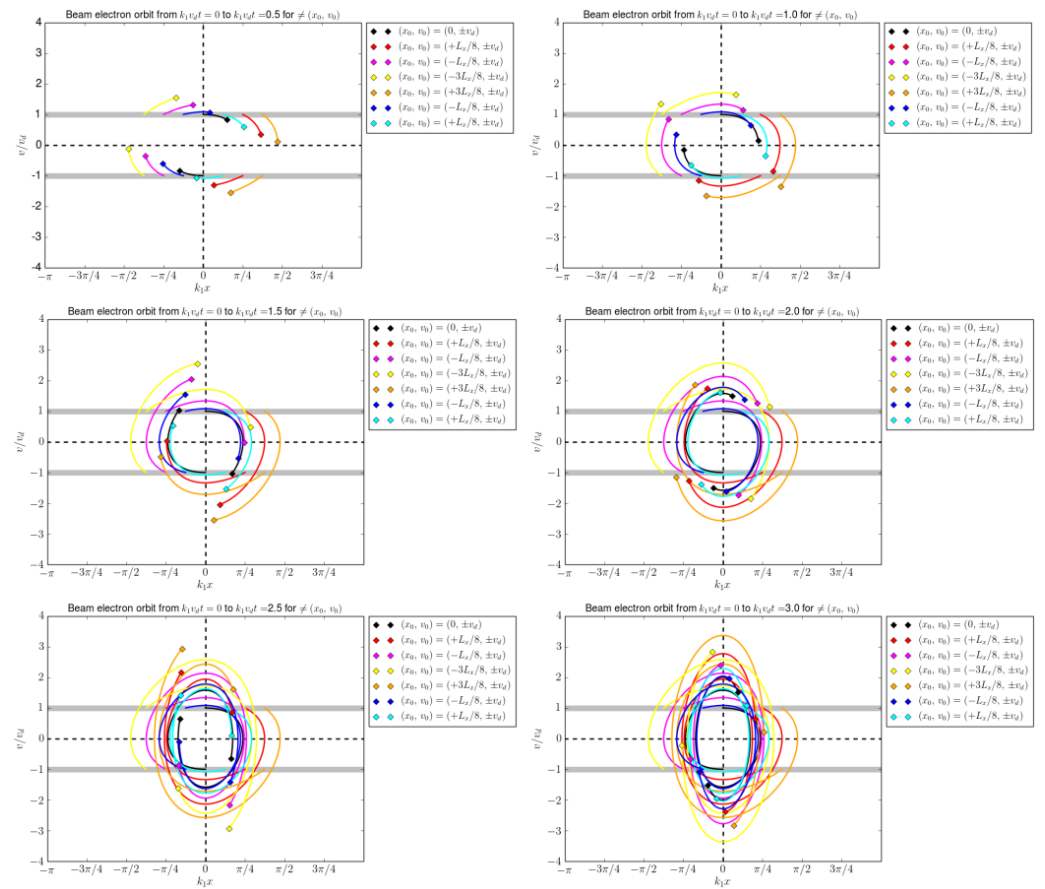


Figure 7: Two stream instability test case : Some beam electron orbits according to the analytical estimates Equation 78 and Equation 79.

References

- Beam, R. M., & Warming, R. F. (1976). An implicit finite-difference algorithm for hyperbolic systems in conservation-law form. *Journal of Computational Physics*, 22(1), 87–110. [https://doi.org/10.1016/0021-9991\(76\)90110-8](https://doi.org/10.1016/0021-9991(76)90110-8)
- Belaiev, S. T., & Budker, G. I. (1956). *Dokl. Akad. Nauk SSSR*, 107.
- Berenger, J.-P. (1994). A perfectly matched layer for the absorption of electromagnetic waves. *Journal of Computational Physics*, 114(2), 185–200. <https://doi.org/10.1006/jcph.1994.1159>
- Bernstein, I. B., Greene, J. M., & Kruskal, M. D. (1957). Exact nonlinear plasma oscillations. *Phys. Rev.*, 108, 546–550. <https://doi.org/10.1103/PhysRev.108.546>
- Bhatnagar, P. L., Gross, E. P., & Krook, M. (1954). A model for collision processes in gases. I. Small amplitude processes in charged and neutral one-component systems. *Phys. Rev.*, 94, 511–525. <https://doi.org/10.1103/PhysRev.94.511>
- Braams, B. J., & Karney, C. F. F. (1987). Differential form of the collision integral for a relativistic plasma. *Phys. Rev. Lett.*, 59, 1817–1820. <https://doi.org/10.1103/PhysRevLett.59.1817>
- Courant, R., Friedrichs, K., & Lewy, H. (1928). Über die partiellen differenzengleichungen der mathematischen. *Physik. Math. Ann.*, 100, 32–74. <https://doi.org/10.1007/BF01532760>

- 363 [10.1007/BF01448839](https://doi.org/10.1007/BF01448839)
- 364 Courant, R., Isaacson, E., & Rees, M. (1952). On the solution of nonlinear hyperbolic differ-
 365 ential equations by finite differences. *Communications on Pure and Applied Mathematics*,
 366 5(3), 243–255. <https://doi.org/https://doi.org/10.1002/cpa.3160050303>
- 367 Crouseilles, N., & Filbet, F. (2004). Numerical approximation of collisional plasmas by high or-
 368 der methods. *Journal of Computational Physics*, 201(2), 546–572. <https://doi.org/https://doi.org/10.1016/j.jcp.2004.06.007>
- 369 <https://doi.org/https://doi.org/10.1016/j.jcp.2004.06.007>
- 370 Dawson, J. (1962). One-dimensional plasma model. *The Physics of Fluids*, 5(4), 445–459.
 371 <https://doi.org/https://doi.org/10.1063/1.1706638>
- 372 de Buyl, P. (2014). The vmf90 program for the numerical resolution of the vlasov equa-
 373 tion for mean-field systems. *Computer Physics Communications*, 185(6), 1822–1827.
 374 <https://doi.org/https://doi.org/10.1016/j.cpc.2014.03.004>
- 375 Debye, P., & Hückel, E. (1923). Zur theorie der elektrolyte. I. Gefrierpunktserniedrigung und
 376 verwandte erscheinungen. *Z. Phys.*, 24, 305–324.
- 377 Decyk, V. K. (1987). Simulation of microscopic processes in plasma. *Proc. 1987 International*
 378 *Conference on Plasma Physics, Kiev, USSR, April 1987, Ed. A G Sitenko [World Scientific,*
 379 *Singapore, 1987] Vol. II, p. 1075.*
- 380 Derouillat, J., Beck, A., Pérez, F., Vinci, T., Chiaramello, M., Grassi, A., Flé, M., Bouchard,
 381 G., Plotnikov, I., Aunai, N., Dargent, J., Riconda, C., & Grech, M. (2018). Smilei :
 382 A collaborative, open-source, multi-purpose particle-in-cell code for plasma simulation.
 383 *Computer Physics Communications*, 222, 351–373. <https://doi.org/https://doi.org/10.1016/j.cpc.2017.09.024>
- 384 <https://doi.org/https://doi.org/10.1016/j.cpc.2017.09.024>
- 385 Duclous, R., Dubroca, B., Filbet, F., & Tikhonchuk, V. (2009). High order resolution of the
 386 maxwell–fokker–planck–landau model intended for ICF applications. *Journal of Computa-*
 387 *tional Physics*, 228(14), 5072–5100. <https://doi.org/https://doi.org/10.1016/j.jcp.2009.04.005>
- 388 <https://doi.org/https://doi.org/10.1016/j.jcp.2009.04.005>
- 389 Fried, B. D., & Conte, S. D. (1961). Elsevier.
- 390 Fromm, J. E. (1968). A method for reducing dispersion in convective difference schemes.
 391 *Journal of Computational Physics*, 3(2), 176–189. [https://doi.org/https://doi.org/10.1016/0021-9991\(68\)90015-6](https://doi.org/https://doi.org/10.1016/0021-9991(68)90015-6)
- 392 [https://doi.org/https://doi.org/10.1016/0021-9991\(68\)90015-6](https://doi.org/https://doi.org/10.1016/0021-9991(68)90015-6)
- 393 Godunov, S. K. (1959). Eine differenzenmethode für die näherungsberechnung unstetiger
 394 lösungen der hydrodynamischen gleichungen. *Mat. Sb., Nov. Ser.*, 47, 271–306.
- 395 Gould, R. W., O’Neil, T. M., & Malmberg, J. H. (1967). Plasma wave echo. *Phys. Rev.*
 396 *Lett.*, 19, 219–222. <https://doi.org/https://doi.org/10.1103/PhysRevLett.19.219>
- 397 Joglekar, A. S., & Levy, M. C. (2020). VlaPy: A python package for eulerian vlasov-poisson-
 398 fokker-planck simulations. *Journal of Open Source Software*, 5(53), 2182. <https://doi.org/https://doi.org/10.21105/joss.02182>
- 399 <https://doi.org/https://doi.org/10.21105/joss.02182>
- 400 Landau, L. D. (1937). *JETP*, 7, 203.
- 401 Landau, L. D., & Lifshitz, E. M. (1981). *Physical kinetics* (Vol. 10). Pergamon Press.
- 402 Lax, P., & Wendroff, B. (1960). Systems of conservation laws. *Communications on Pure*
 403 *and Applied Mathematics*, 13(2), 217–237. <https://doi.org/https://doi.org/10.1002/cpa.3160130205>
- 404 <https://doi.org/https://doi.org/10.1002/cpa.3160130205>
- 405 Liu, X.-D., Osher, S., & Chan, T. (1994). Weighted essentially non-oscillatory schemes.
 406 *Journal of Computational Physics*, 115(1), 200–212. <https://doi.org/https://doi.org/10.1006/jcph.1994.1187>
- 407 <https://doi.org/https://doi.org/10.1006/jcph.1994.1187>
- 408 Roe, P. L. (1986). Characteristic-based schemes for the euler equations. *Annual Review of*
 409 *Fluid Mechanics*, 18(1), 337–365. <https://doi.org/https://doi.org/10.1146/annurev.fl.18.010186.002005>

- 410 Rosenbluth, M. N., MacDonald, W. M., & Judd, D. L. (1957). Fokker-planck equation for
411 an inverse-square force. *Phys. Rev.*, 107, 1–6. <https://doi.org/10.1103/PhysRev.107.1>
- 412 Sagdeev, R. Z., & Galeev, A. A. (1969). *Nonlinear Plasma Theory*. W. A. Benjamin, Inc.,
413 New York.
- 414 Touati, M., Feugeas, J.-L., Nicolai, P., Santos, J. J., Gremillet, L., & Tikhonchuk, V. T.
415 (2014). A reduced model for relativistic electron beam transport in solids and dense
416 plasmas. *New Journal of Physics*, 16(7), 073014. [https://doi.org/10.1088/1367-2630/](https://doi.org/10.1088/1367-2630/16/7/073014)
417 [16/7/073014](https://doi.org/10.1088/1367-2630/16/7/073014)
- 418 Tzoufras, M., Bell, A. R., Norreys, P. A., & Tsung, F. S. (2011). A vlasov–fokker–planck code
419 for high energy density physics. *Journal of Computational Physics*, 230(17), 6475–6494.
420 [https://doi.org/https://doi.org/10.1016/j.jcp.2011.04.034](https://doi.org/10.1016/j.jcp.2011.04.034)
- 421 van Leer, B. (1979). Towards the ultimate conservative difference scheme. V. A second-
422 order sequel to godunov's method. *Journal of Computational Physics*, 32(1), 101–136.
423 [https://doi.org/https://doi.org/10.1016/0021-9991\(79\)90145-1](https://doi.org/10.1016/0021-9991(79)90145-1)
- 424 Van Leer, B. (1977). Towards the ultimate conservative difference scheme III. Upstream-
425 centered finite-difference schemes for ideal compressible flow. *Journal of Computational*
426 *Physics*, 23(3), 263–275. [https://doi.org/https://doi.org/10.1016/0021-9991\(77\)](https://doi.org/10.1016/0021-9991(77)90094-8)
427 [90094-8](https://doi.org/10.1016/0021-9991(77)90094-8)
- 428 Vlasov, A. A. ;. (1938). *JETP*, 8(3), 291.
- 429 Yee, K. (1966). *IEEE Transactions on Antennas and Propagation*, 14(3), 302–307. <https://doi.org/10.1109/TAP.1966.1138693>
430